Advances in Science and Technology Research Journal

Advances in Science and Technology Research Journal, 18(8), 56–72
https://doi.org/10.12913/22998624/192699
ISSN 2299-8624, License CC-BY 4.0

Received: 2024.08.20
Accepted: 2024.09.20
Published: 2024.11.01

Analysis of the Operating Conditions of the ASz-62IR Engine During Flight

Piotr Jakliński[1], Jacek Czarnigowski[1], Karol Ścisłowski[1*]

[1] Department of Thermodynamics, Fluid Mechanics and Aircraft Propulsion Systems, Lublin University of Technology, Poland

* Coresponding author's e-mail: k.scislowski@pollub.pl

ABSTRACT

The article describes the results of an analysis of the states and operating conditions the ASz-62 IR-16E engine. The tests were carried out on an AN-2 aeroplane with the ASz-62IR-16E engine. The purpose of this study was to determine the contribution of static and dynamic engine operating states during flight. The engine operating parameters were recorded at a frequency of 16 Hz for over 7 hours of flight. The engine operating points defined by two parameters, i.e. engine speed and intake manifold pressure were analysed, and the mean values, standard deviations and histograms of the distributions of these parameters were determined. The distribution of the occurrence of various operating states, i.e. steady states and transients was also analysed for low, medium and high load, and for IDLE and WOT. The article describes the contribution of the individual engine operating states to the total flight time. The results obtained for the aircraft engine are compared with those obtained for automotive vehicle engines and described in the paper. The study shows that most of the operating time of the ASz-62IR-16E aircraft engine was in steady-state conditions – about 90% of this time, whereas steady-state operating conditions for the automotive engine account for about 80% of the driving time. For the aircraft engine, more than 65% of operating time is heavy load. Small and medium loads account for 10% and 25% of operating time, respectively. In the case of the car engine, only about 5% of operating time is heavy load, while the major part of operating time is under light (about 40%) and medium (about 55%) load. Under idling conditions, the aero-engine's operating time was about 6.2%, i.e. about twice shorter than that of the car engine (about 13.2%). Under WOT conditions, the aircraft engine had an operating time of 1.3%, while for the car engine this condition was extremely rare – about 0.1%. It was also shown that the ASz-62IR-16E aircraft engine of the AN-2 aircraft in real flight conditions has a specific, most frequently used operating point lying in the range of the values: n = 1800 ÷ 1900 RPM and MAP = 0.8 ÷ 0.95 Bar.

Keywords: airplane, aircraft engine, flight analysis, engine operating conditions.

INTRODUCTION

Despite the continuing development of aircraft turbine engines and their increasing use in aircraft propulsion, piston engines are still widely used even in newer aircraft designs [1]. They still show many advantages over turbine engines [2]. Low inertia giving the possibility of a rapid change in operating conditions, easy starting, the low weight and size of piston engines or ease of servicing [3] are just some of the advantages of their use for aircraft propulsion. Their advantages are particularly noticeable in aircraft flying in variable conditions and at low altitudes. Examples include aerobatic, tourist, training, agricultural or fire-fighting aircraft. Piston drives are, therefore, likely to be used in these branches of aviation for a long time to come, and this makes it constantly profitable to develop and improve their designs [4, 5]. Aviation is not subject to such stringent emission standards as, for example, automotive transport [6]. This results in many units, even in new aircraft, being powered by carburettor systems [7]. In addition, the engines themselves are often only development versions of older designs, which provides ample scope for changes and improvements to the engines themselves as well as to the associated systems and systems [8, 9].

The optimum operating characteristics of an aircraft engine power system may not be universal for all flight phases and conditions [10, 11]. During take-off or climb, it is usually expected to achieve maximum engine power without overloading the engine structure, while in steady-state flight it is expected to achieve the greatest efficiency of the propulsion system and thus minimise fuel consumption [12, 13]. When designing and selecting aircraft propulsion system components, it is very important to determine the operating conditions of the aircraft [14]. Aircraft engine operating conditions can be specified by recording the most important parameters of the aircraft propulsion system during a flight simulating the conditions of standard operation of the aircraft in question. Measurements can be made by installing appropriate measurement instrumentation or via on-board diagnostic equipment [15]. From the collected data, it is possible to determine the average engine loads in individual flight phases [16], the share of individual engine operating states over the entire period of operation as well as the share of steady and transient states [17].

In recent years, the share of electric drives in transport has noticeably increased [18]. This applies not only to automotive transport. Such an electrification trend is noticeable in smaller vehicles such as motorbikes and scooters [19], and also in aviation [20]. Currently, electric aeroplane propulsion is a market novelty and is mainly used in motorised gliders [21] and unmanned aircraft, although work is also being carried out to apply it to large aircraft [22, 23]. The main limitation to the use of electric propulsion in aviation is a low density of electricity stored in batteries compared to conventional aviation fuel [24]. It can be assumed that with the development of batteries, electric aircraft will become increasingly popular [25, 26]. Work is currently underway to apply hybrid propulsion systems to aviation [27, 28]. The electric motor could provide an additional source of power in conditions of the highest power requirements and simultaneously batteries could be recharged on the ground or during flight when the internal combustion engine is able to cover the entire power demand. The concept of hybrid drives is already very popular in land transport. The solutions currently in use are proven, refined and reliable. The implementation of some of the solutions and components familiar from cars is possible, but it must be remembered that aircraft propulsion systems operate under extremely different conditions [29, 30]. Although many research results describing the operating conditions of car propulsion systems under different operating conditions are available [31], there are few works describing the operating conditions of an aircraft engine. The works [32, 33] show that the application of hybrid propulsion in aviation can bring tangible benefits, but if a properly functioning system is to be built and controls are to be determined, it is necessary to determine the operating conditions of the propulsion system.

METHODOLOGY AND RESEARCH OBJECT

Research object

The object of the research was an AN-2 aircraft with a registration number SP-ZET, belonging to WSK PZL-Kalisz S.A., the largest Polish manufacturer of ASz-62IR aircraft engines. It is a biplane used for aeroclubs, transport or agricultural applications. The aircraft used for the study is shown in Figure 1.

The aircraft is driven by the ASz-62IR-16E radial engine (Figure 2). This design is based on the ASz-62IR engine and extended with an electronic fuel injection control system with Type Certificate No. EASA.E.140 [34]. The engine specifications are shown in Table 1.

Scope of the research

The tests were aimed at determining the basic performance of the aircraft's propulsion system under normal operating conditions. The measurements were made during certification tests to adapt the aircraft design to the new engine type. The recording of propulsion system performance parameters did not require the installation of additional measurement instrumentation. The data was processed by the engine controller, and a PC connected to the engine controller via a diagnostic connector recorded the data. The following parameters were recorded:

- crankshaft speed – RPM, min^{-1}
- intake manifold pressure – MAP, kPa.

The data was recorded at a frequency of 16 Hz. During the four flights, a data sequence containing 390.701 measurement points (Table 2) was recorded for a total time of 7 h and 4 min.

Figure 1. AN-2 aircraft used for testing

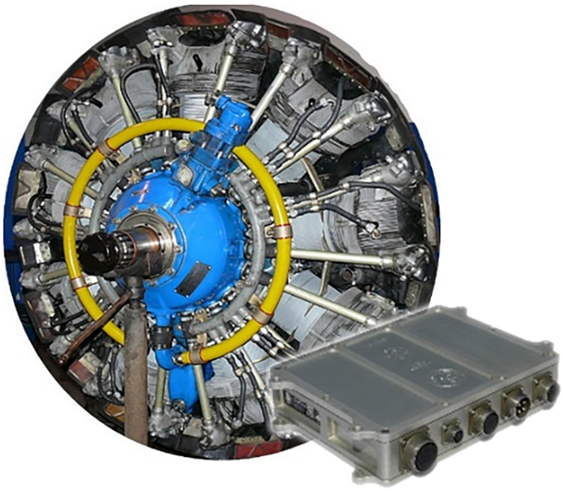

Figure 2. ASz-62IR-16E engine

Table 1. Technical data for the ASz-62IR-16E [35]

Type	R9, 9-cylindrer, radial
Cooling system	Air-cooled
Length	1328 mm
Diameter	1380 mm
Dry weight	579 kg + 2%
Displacement	29.87 dm^3
Bore	155.5 mm
Stroke – cylinder nr 1	174.5 mm
Compression ratio	6.4 ± 0.1
Power-to-weight ratio	1.25 kW/kg
Supercharger	Single stage, single speed, geared centrifugal supercharger
Gear ratio	0.6875
Fuel types	100LL, OBR 85 UL
Fuel system	Electronically controlled multipoint fuel injection system
Oil system	Dry sump
Power / RPM / MAP (take-off)	721 kW / 2200 min^{-1} / 140 ± 3 kPa
Power / RPM / MAP (rated)	605 kW / 2100 min^{-1} / 120 ± 1 kPa
RPM idle min	550 min^{-1}
RPM max	2200 min^{-1}
Specific fuel consumption (take off)	> 300 g/kWh
Specific fuel consumption (0.5 Power rated)	~220 g/kWh

Methodology

In order to determine the basic operating conditions of the ASz-62IR engine in real use, it was decided to analyse three issues: in the first one (A), the engine operating time was determined at low, medium and high load; in the second one (B) – the engine operating time at IDLE and at WOT; and in the third one (C) – the total engine operating time under steady-state and transient conditions.

The analysis was carried out for the data collected from all four flights. The data was first filtered in order to negate the influence of signal noise, individual measurement errors and the limited measurement resolution of the system. Moving-average signal filtering was applied. The filter length N was selected from an analysis of the second time derivative of the speed for several selected operating intervals. The filter length was considered sufficient if, in the intervals acceleration or deceleration occurred the second derivative of the speed did not oscillate between positive and negative values. The courses of the first and second derivative for different filter lengths are shown in Figure 3.

It was decided that it would be optimal to use a filter of length N = 8. In this case, each measurement point obtained would be the average of a 0.5 s time interval. Figure 4 shows the effect of filtering the time interval of the engine speed signal.

Table 2. Data recorded during the test flights [19]

No.	Start date	Measuremet time	Number of measurement points
1	2020-08-06 14:06:11	4983.78	76 512
2	2020-08-12 14:13:39	8198.59	125 481
3	2020-08-13 13:35:07	7037.22	108 622
4	2020-09-09 15.42.27	5215.00	80 086

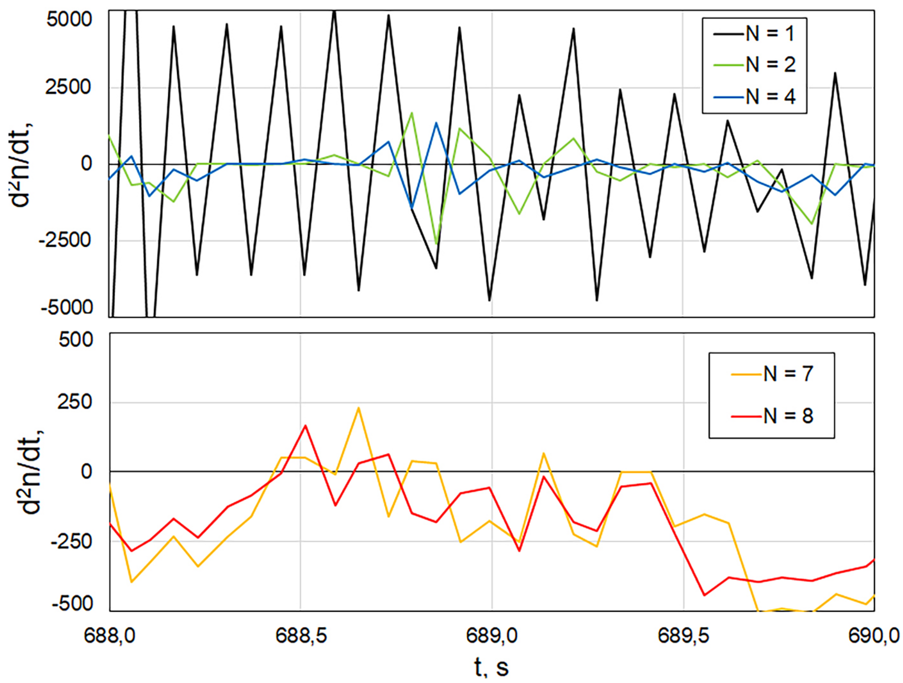

Figure 3. Second derivative of the speed for different filter lengths

The analysis of the load conditions of the aircraft engine was based on the rotational speed - n and the intake manifold pressure value – MAP. As in the other work [36], three engine operating states were therefore distinguished and determined: low load, medium load and high load (Figure 5). In addition, IDLE and WOT were also determined. The values of these categories are shown in Fig. 5 and Table 3. The minimum idling speed RPMmin = RPMidlemin = approx. 550 min^{-1} was taken as the start of the interval. The end of the interval was defined as the maximum permissible speed for the engine: RPMmax = 105% RPMrated = 2200 min^{-1} [28]. MAPmin was taken as the minimum idle pressure MAPidlemin = ~30 kPa and MAPmax the maximum allowable charging pressure ~140 kPa. The lower and higher RPM values were taken as overruns and the lower MAP values as engine braking. RPM 100% and MAP 100% represent RPMrated and MAP respectively for RPMrated = MAPrated. The RPM and MAP ranges thus selected were divided according to: < 30%, 30–70% and > 70%, and the areas defined in the paper as low, medium and high load were determined in this way (Figure 6). The IDLE area does not exceed 900 min^{-1} and 35 ÷ 50 kPA, and WOT was

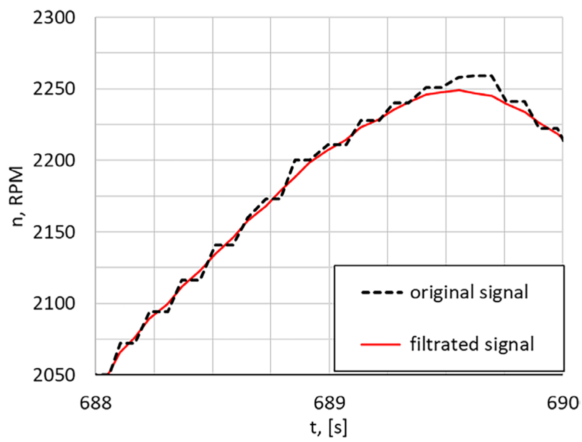

Figure 4. Input signal and signal after filtering

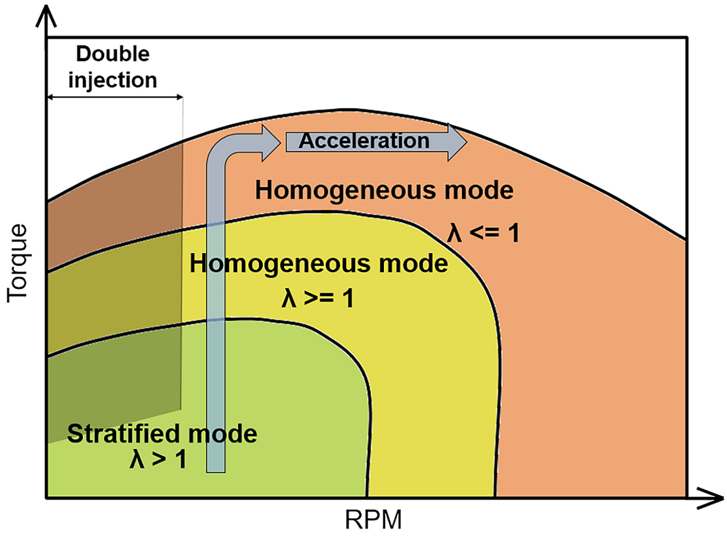

Figure 5. Sample strategy to control the SI engine [37]

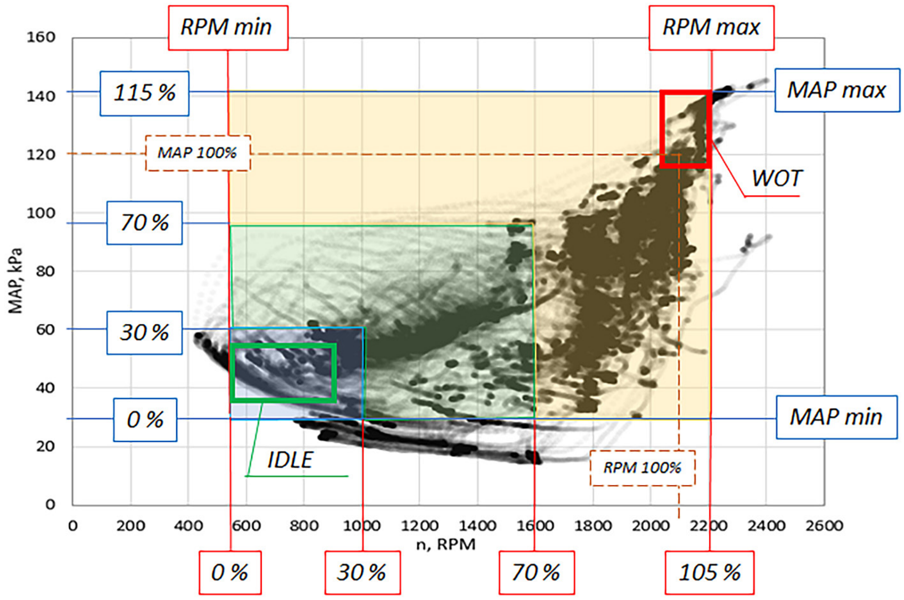

Figure 6. Distinct engine operating areas superimposed on the measuring points

defined above 2060 min^{-1} and 118 kPa (Table 3). In order to determine the contribution of steady-state and transient engine operating conditions, it was necessary to determine which conditions would be classified as steady-state and transient.

Undetermined operating conditions can be determined by the following parameters:

- average duty cycle indexed pressure – p_i,
- instantaneous engine torque – M_o,
- crankshaft speed – n,
- total heat flow through the engine – $\dot{Q}$.

Theoretically, the operating condition of an internal combustion engine can be defined as a steady state if the following conditions are met:

$$\frac{dM_o}{dt}=0\,;\ \frac{dn}{dt}=0\,;\ \frac{d\dot{Q}}{dt}=0;\ \frac{dp_i}{dt}=0 \qquad (1)$$

In reality, meeting these conditions is impossible. It is also difficult to record all the parameters mentioned. Transients are therefore determined using selected parameters and taking individual limits of the time derivative.

For the purposes of this study, the determination of transients was based on an analysis of the time variation of the engine speed.

For this purpose, its time derivative was specified. The determination of the RPM variation intervals made it possible to determine the contribution of steady-state and dynamic operating

Table 3. Areas of the specified engine operating states

Engine operating state	RPM	MAP
Low load	0 ÷ 30% RPM_{rated} ~ (550 ÷ 1000) min^{-1}	0 ÷ 30% MAP_{rated} ~ (30 ÷ 60) kPa
Medium load	30 ÷ 70% RPM_{rated} ~ (1000 ÷ 1600) min^{-1}	30 ÷ 70% MAP_{rated} ~ (60 ÷ 95) kPa
High load	70 ÷ 105% RPM_{rated} ~ (1600 ÷ 2200) min^{-1}	70 ÷ 115% MAP_{rated} ~ (95 ÷ 140) kPa
IDLE	0 ÷ 20% RPM_{rated} ~ (550 ÷ 850) min^{-1}	0÷20% MAP_{rated} ~ (30 ÷ 50) kPa
WOT	98 ÷ 105% RPM_{rated} ~ (2060 ÷ 2200) min^{-1}	98 ÷ 115% MAP_{rated} ~ (118 ÷ 140) kPa

conditions over the entire engine operating time studied (Figure 7). The engine operating points were defined as transient operating conditions with the change in speed per second greater than 1% of the RPMmax of 2200 min^{-1} for this engine:

$$\left|\frac{\delta n}{\delta t}\right| \geq \frac{n_{max}}{t} \cdot 1\% \qquad (2)$$

Figure 8 shows an example of the time course of *RPM* and *MAP* intake manifold pressure during the analysed flight. The specified engine operating states are marked in green

ANALYSIS OF RESULTS

A – Motor load

A 3D histogram for RPM and MAP was drawn from all the measurement points obtained (Fig. 9). This graph shows the percentage of the engine operating time at a given point/area determined by (RPM_MAP) relative to the total engine operating time. The overlaid on the 3D histogram shows the areas corresponding to the predefined engine operating states.

It is clear from the distribution/chart that most of the engine operating points fall into two characteristic areas: the first, smaller ones lie in the low load area and the second, larger ones in the high load area. In the medium load area, on the other hand, far fewer measuring points are recorded. In addition, there are areas of the engine operation that lie outside the described/defined load areas. One of these is a small area for RPM 2200 ÷ 2300 min^{-1} and pressure above 140 kPA. This is the result of exceeding the speed and pressure limits when the engine is at its maximum performance. This area represents 0.97% of the total engine operating time. The second is the area below 30 kPA and can be identified with engine braking when

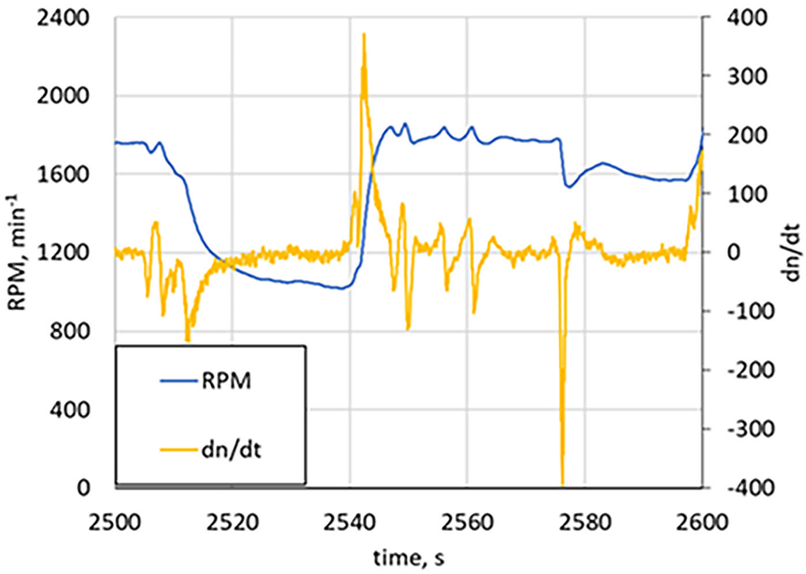

Figure 7. The course of the engine speed RPM and its time derivative dn/dt during a sudden increase in throttle opening

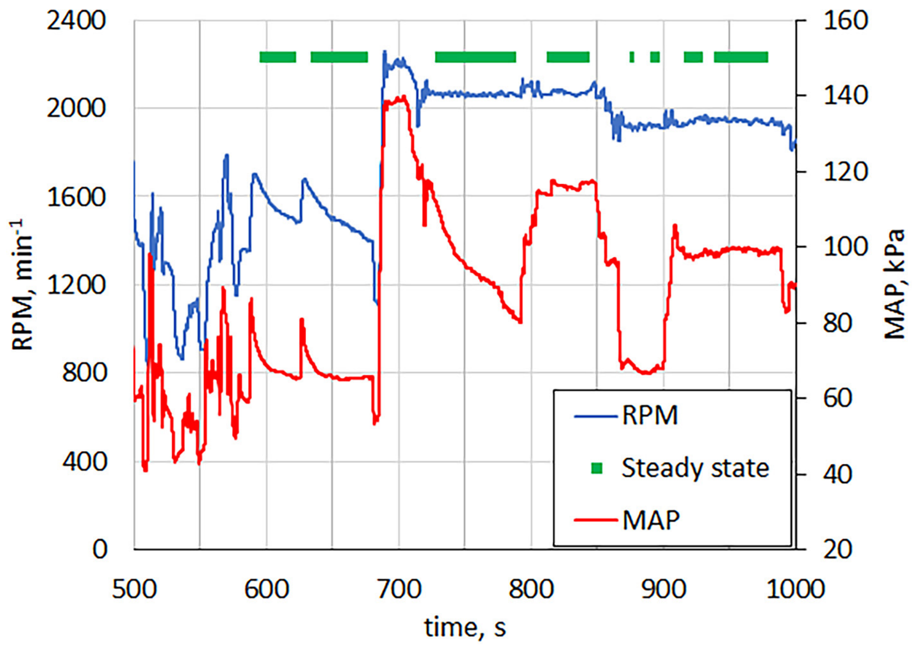

Figure 8. Time course of the intake manifold speed and pressure during flight

the engine throttle is closed. It represents 3.5% of the operating time. As seen in the 3D figure (Fig. 9), the engine was most often operating in the area defined as high load. This is by far the largest area on the graph that accounts for 66.31% of the engine's total operating time. The second such area frequently used by the engine is the area defined as low load where two characteristic spots can be seen. This area represents 14.96% of the total engine operating time.

In the area defined as medium load (RPM 1000 ÷ 1600 min^{-1} and MAP 60 ÷ 95 kPa), it is difficult to find any characteristic places of engine operation. It seems to be a transition area between low and high load conditions and represents 15.21% of the total engine operating time.

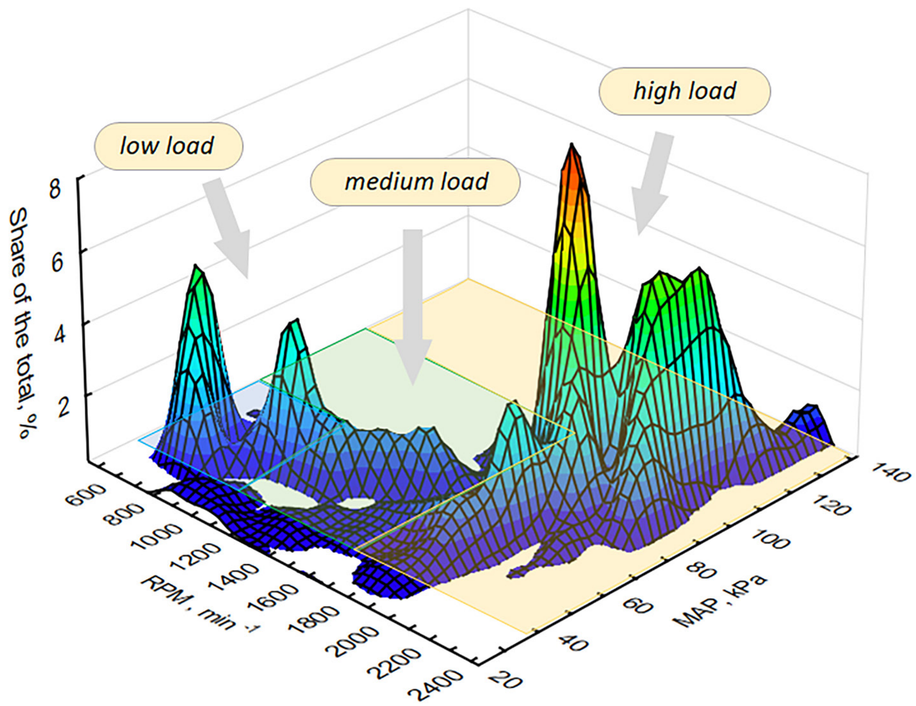

Figure 9. 3D histogram of the ASz-62IR-16E aircraft engine performance - flight test averaged data

The other areas of the diagram defined as overruns and engine braking represent a marginal part of the diagram area. The overrun of permissible speeds and pressures (RPM < RPMmin and RPM > RPMmax) are included in the operating time calculations for low and high load, respectively. In contrast, the engine braking area is not included in these calculations.

The areas of most frequent engine operation described above can also be seen and confirmed in the 2D figure (Fig. 10). It clearly shows a characteristic density of the measurement points for the engine operation around the point RPM~600 min^{-1} and MAP~40 kPA for low load and a second higher density of the points around the point RPM~1800 min^{-1} and MAP~90 kPA for high load. The first of these densities most likely represents idle and the second the most commonly used engine operating condition during flight. The diagram also shows the propeller characteristics of this engine, marked with a dashed line.

B – IDLE and WOT

IDLE

In the case of idling, it is possible to distinguish two local extremes. The first, noticeable for RPM~900 min^{-1} and MAP~50 kPA is the idle for a cold engine, while the second, larger one, noticeable for RPM~650 min^{-1} and MAP~40 kPa is the idle for a warm engine. In addition, a group of points can be seen in Fig. 11 forming the idle curve the engine clearly tends towards after returning from engine braking. Engine braking can also be seen in the form of a group of curves below 30 kPA ending at around 800 min^{-1}.

The idling limits defined in the paper are shown as a green rectangle on the graph (Fig. 11). It can be seen that during the measurements, the engine was running at RPM < RPM min, resulting in an increase in MAP above 50 kPa. These speeds were up to 430 min^{-1} with a MAP close to 60 kPA. In the calculation of operating time at IDLE, these overruns were also taken into account and added to IDLE. In contrast, the operating time at 900 min^{-1} and 50 kPA defined as IDLE for a cold engine was not included. The IDLE defined in this way represents more than 8% of the total engine operating time.

WOT

For the full load case, two local extremes can also be distinguished (Fig. 12). The first (marked as W1) for RPM < 2150 min^{-1} and MAP < 120 kPa can be identified with the maximum sustained power probably used for climb, and the second for RPM > 2150 min^{-1} and MAP > 120 kPA can be identified with take-off power.

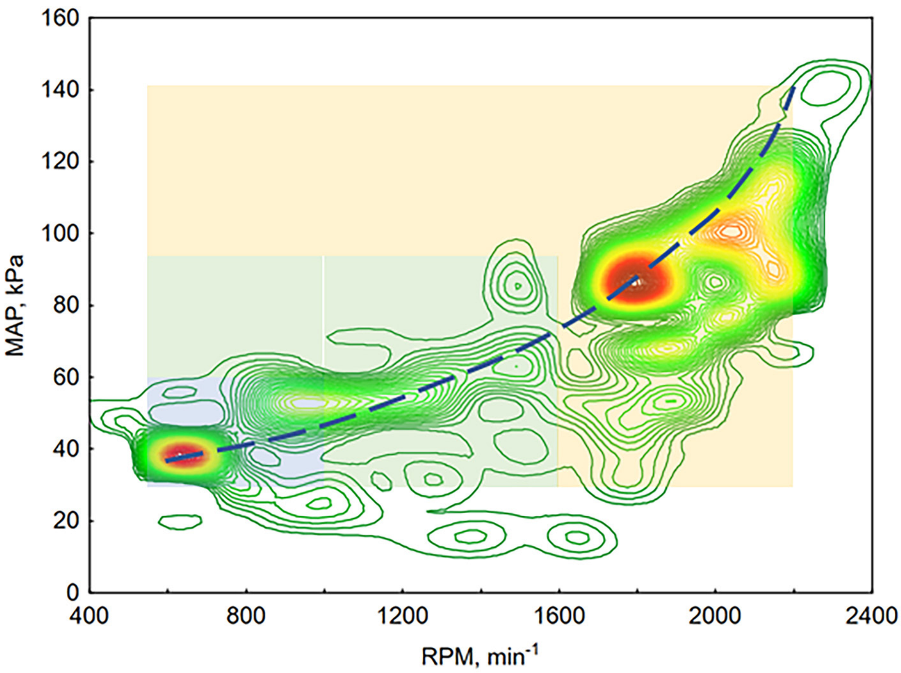

Figure 10. 2D histogram of all engine operating points with the propeller characteristics superimposed

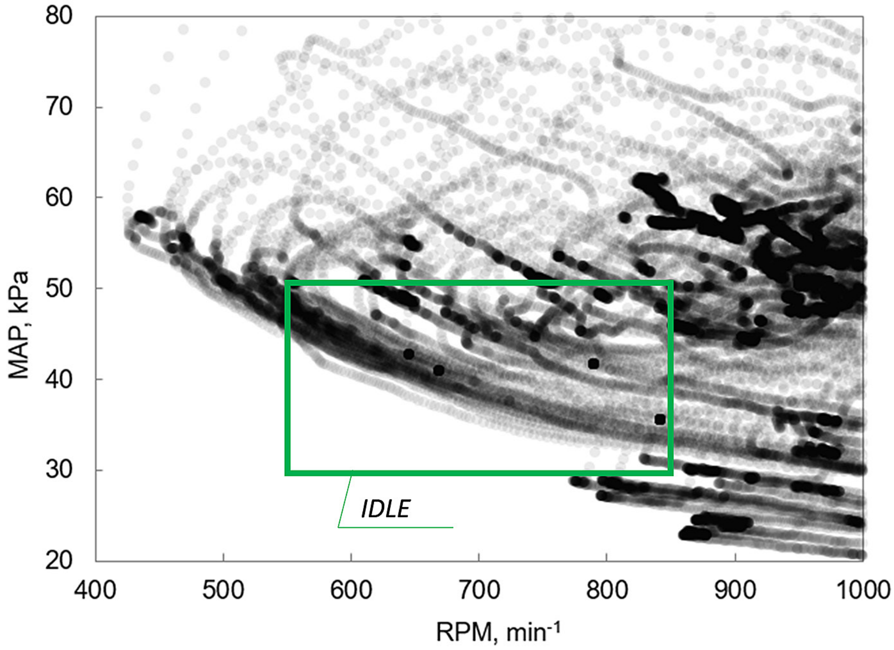

Figure 11. Engine operating point range defined as IDLE

In the case of take-off power, exceedances of the allowed maximum RPM can also be observed. RPM exceedances reach 2280 min^{-1} and even occasionally up to 2400 min^{-1}. These are points outside the upper right corner of the red rectangle that defines the WOT limits adopted in the work. In the calculation of the WOT working time, the above exceedances were also taken into account and added to the WOT. The WOT so defined represents 2.34% of the total engine operating time. In the case of starting power, two areas can also be distinguished. One is the area with RPM ~2170 min^{-1} and MAP 115 ÷ 138 kPA labelled W2 and the other labelled W3 for RPM >2180 min^{-1} and MAP >138 kPA which can be referred to as the take-off power maximum. This can be seen around the upper right corner of the red rectangle that defines the WOT limits adopted in the work.

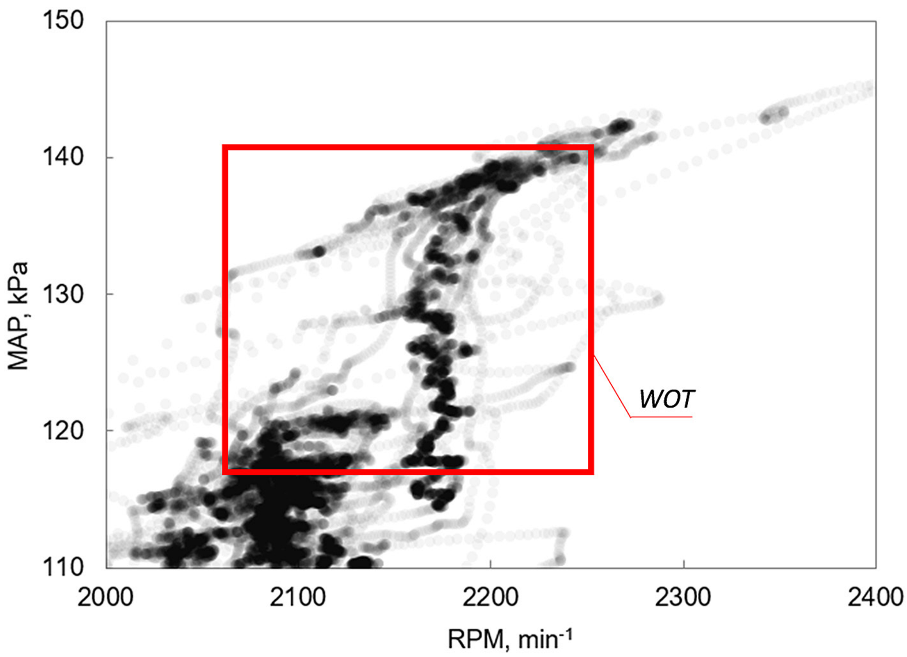

Figure 12. Range of the engine operating points defined as WOT

The take-off power extreme (W3) identified in this way is only 108 seconds out of ~24400 s of the flight record and represents about 0.44% of the total operating time. Dividing this into 4 flights (take-offs) means that maximum take-off power is only used for less than 30 seconds per flight.

C – Steady and transient states

The analysis of the variability of the engine operating conditions was based on the time derivative of the rotational speed (RPM) and the intake manifold pressure (MAP). A histogram of the RPM variation is shown in Figure 13. From this parameter, the proportion of steady-state and transient engine operating states was determined. For more than 90% of the flight time, the speed variation was no more than 24 RPM/s.

Figure 14 shows a histogram of the variation in intake manifold pressure (MAP). As in the case of speed, the low variability of the parameter considered is noticeable. For 62.1% of the flight time, the variability of the MAP parameter did not exceed 0.4 kPa/s.

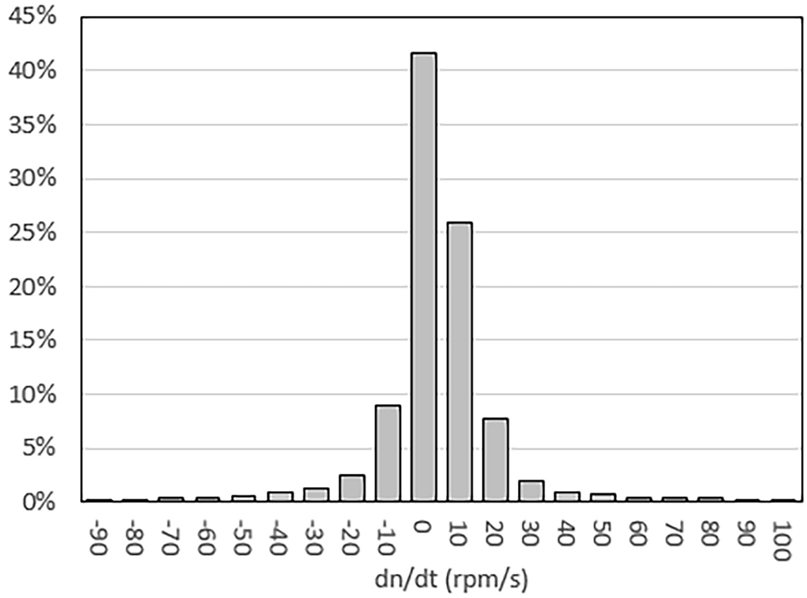

Figure 13. Histogram of the speed variation during flight

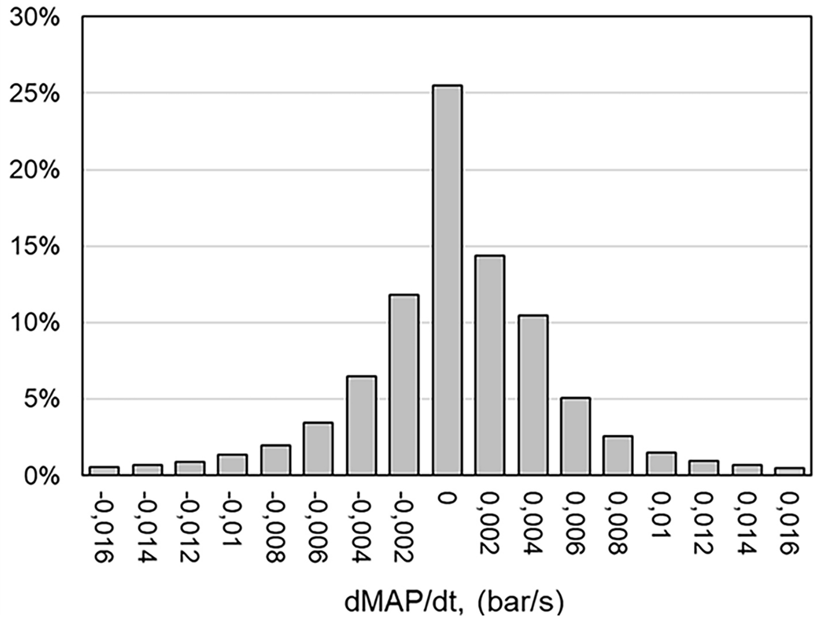

Figure 14. Histogram of the inlet manifold pressure variation during flight

According to a predefined definition of engine transients, they were determined to account for 9.98% of the total flight time. A distinction was also made between transient states of operation into acceleration when the engine speed is increased and deceleration when the speed is decreased (deceleration, engine braking). The ranges of the division of the different states and their percentage contribution during flight are shown in Table 4 and Figure 15.

It can be seen from the data that engine operation mostly occurred in the states defined as steady. Fig. 16 shows a histogram of the intake manifold pressure and speed for an engine operating exclusively in steady states. It is clear that these states are characteristic 'islands' in the figure. They denote areas the engine does not significantly change its operating parameters over a long period of time. The largest and most steady states can be seen at high loads (RPM 1700 ÷ 2100 min^{-1} and MAP 60 ÷ 120 kPa) and around low loads (RPM 5000 ÷ 1000 min^{-1} and MAP 30 ÷ 55 kPa). The areas of RPM ~1900 min^{-1} and MAP ~60 kPa and RPM ~2100 min^{-1} and MAP ~90 kPa are points of flight with a slight descent (decreasing altitude). For the medium loads (middle of the graph), steady states account for a much smaller share and even their occurrence is marginal.

Figure 17 shows a histogram of the two variables for positive transients. These states are associated with increasing engine speed. As can be seen in the figure, they occur most frequently for RPM (1000 ÷ 1400 min^{-1}, followed by 1700 ÷ 1900 min^{-1} and then 2000 ÷ 2100 min^{-1}). These areas therefore show the areas of most frequent engine acceleration and mostly line up with the propeller-like characteristics. The area of RPM ~1900 min^{-1} and MAP ~ 60 kPa seems to be the point of onset of acceleration after a slight descent (decreasing altitude).

Figure 18 shows a histogram of the two variables including negative transients. These states are associated with deceleration (decreasing

Table 4. Transient states of engine operation

Parameter	Range of the time derivative of speed	Share of the given operating states
Acceleration	$\frac{\delta n}{\delta t} > 24\ \frac{RPM}{s}$	4.75%
Deceleration	$\frac{\delta n}{\delta t} < -24\ \frac{RPM}{s}$	5.23%
Total		9.98%

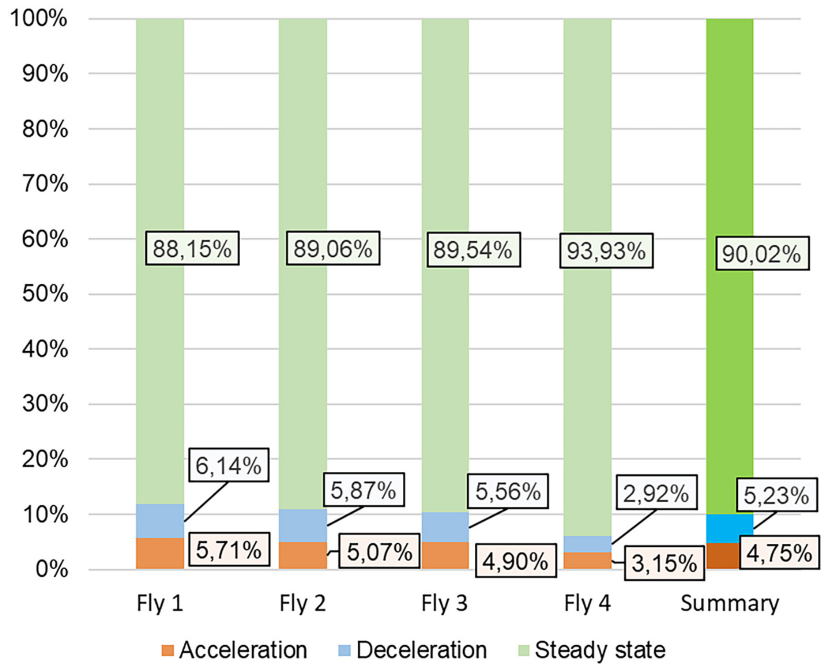

Figure 15. Percentage of aircraft engine operating states during individual flights

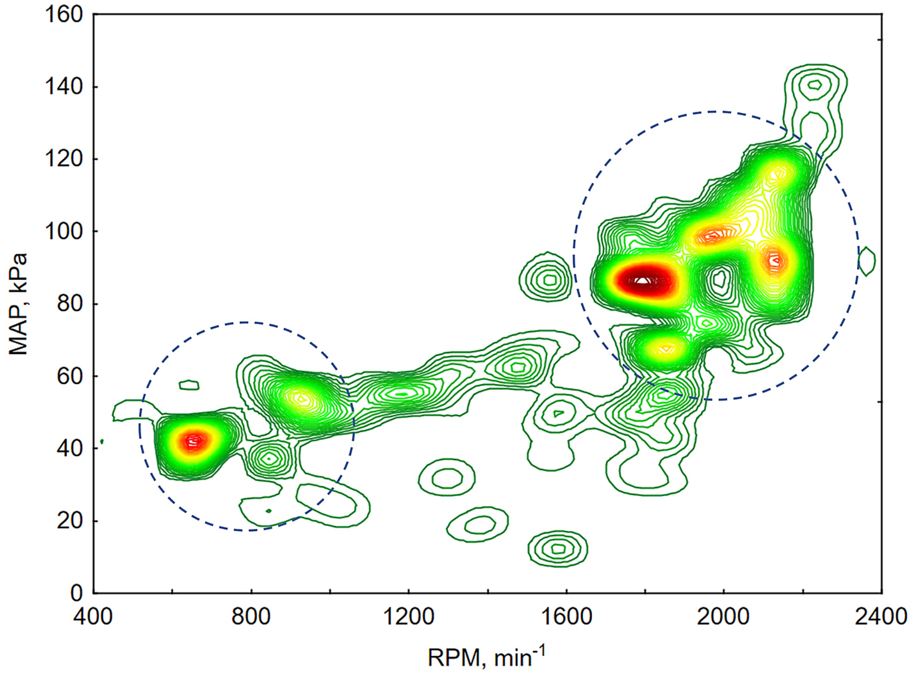

Figure 16. Histogram of two variables – speed and manifold pressure for fixed engine operating points only

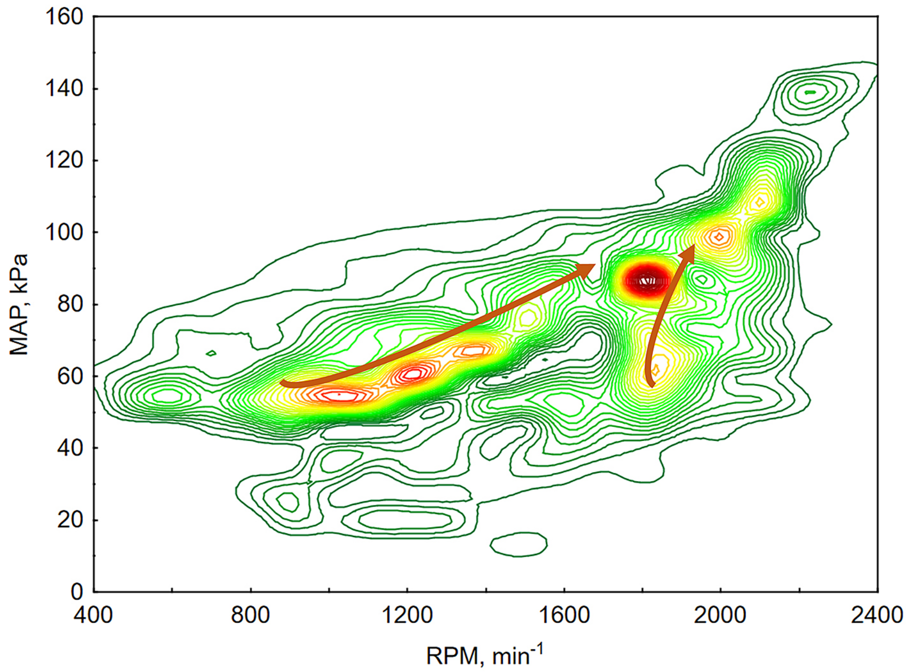

Figure 17. Acceleration – histogram of the manifold velocity and pressure for only the transient operating points of the engine at which the speed was increased

RPM). As can be seen in the figure, they occur most frequently for RPM (2100 ÷ 2000 min^{-1}, then 1900 ÷ 1700 min^{-1}, 1300 ÷ 1100 min^{-1}, and 700 ÷ 500 min^{-1}). They are located along a single line and represent the areas of the most frequent engine RPM deceleration, i.e. the operating states the engine load significantly decreases. In addition, it is possible to find a deceleration area (RPM 1900 ÷ 1500 min^{-1}) with descending from the operating point of RPM ~1800 min^{-1} and MAP ~85 kPa, and the area of RPM 1600 ÷ 800 min^{-1} and MAP 20 ÷ 30 kPa which is responsible for engine deceleration, i.e. reducing engine speed when the throttle is closed.

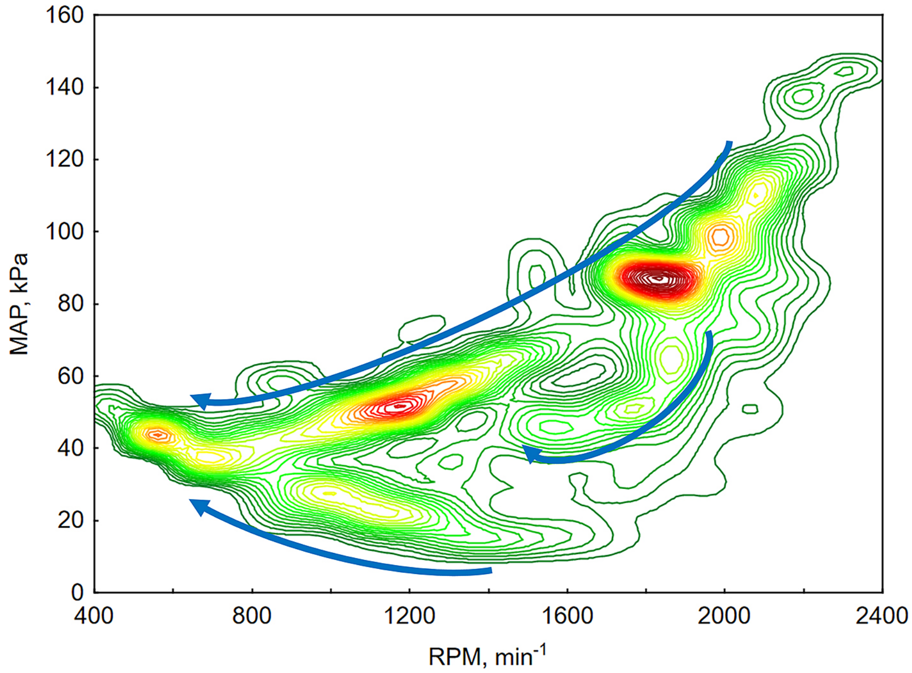

Figure 18. Deceleration – histogram of the manifold velocity and pressure for only the transient operating points of the engine at which the speed was reduced

DISCUSSION

The paper presents an analysis of the operating conditions of an aircraft engine operating under short test flight conditions (Figure 19) and compares the results of the performance of an engine powering a motor vehicle under urban operating conditions (Figure 20) [38].

During flight, the ASz engine operated mainly in the high RPM>1600 min^{-1} range (> 70% RPMrated) under medium to high MAP > 75 kPa (> 50% MAPrated). The most common operating point is in the range of 1700 ÷ 1900 min^{-1} and 75 ÷ 95 kPa, which is ~80% RPMrated and ~65% MAPrated. The average intake manifold MAP pressure was 73 kPA (~50% MAPrated). This

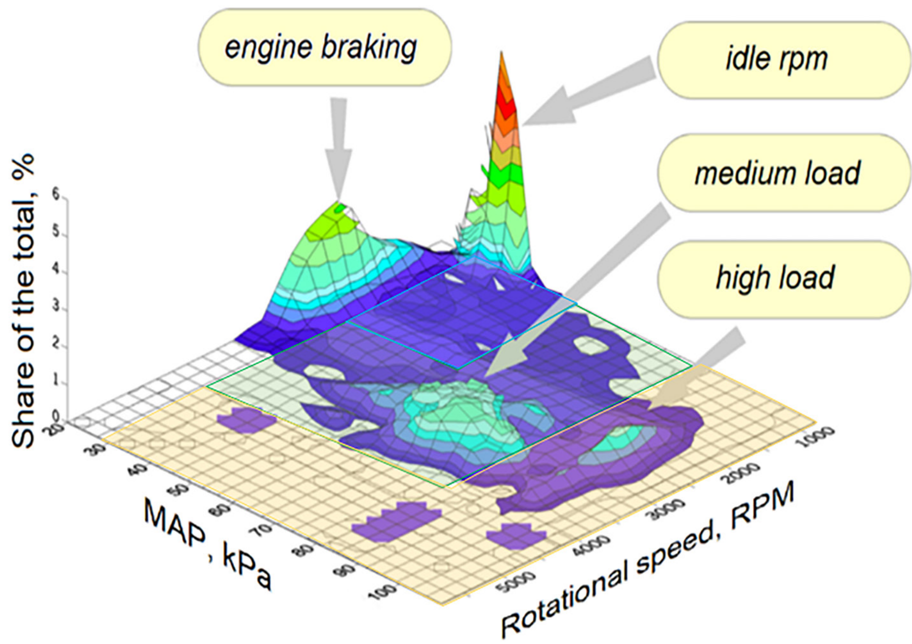

Figure 19. 3D histogram of the ASz-62IR engine operating conditions

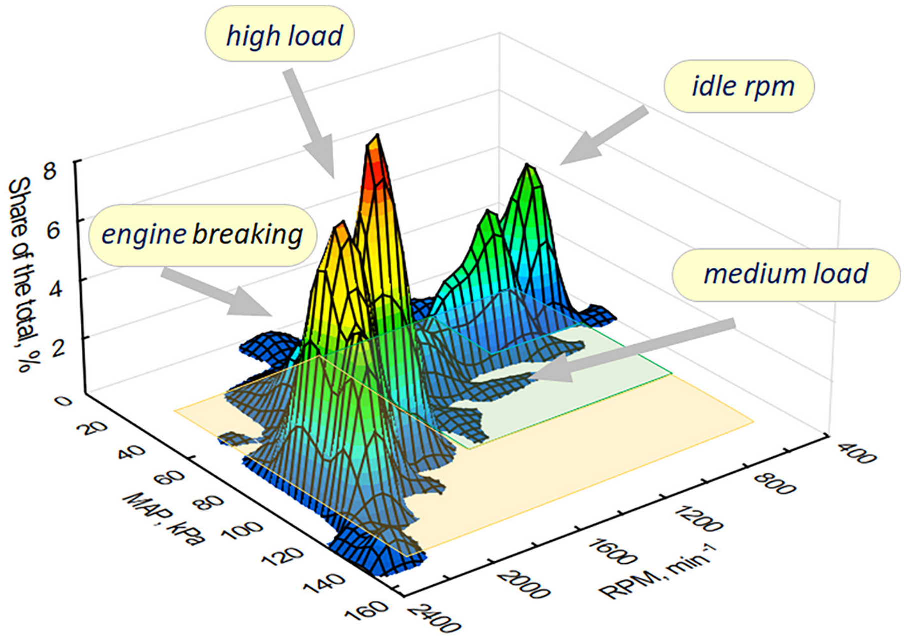

Figure 20. 3D histogram of the automotive engine operation under operating conditions [38]

means that, for an aero engine, more than 66.3% of the operating time is heavy load (Figure 21). The low and medium loads account for 15.0% and 15.2% of the operating time, respectively.

The high RPM of automotive engines (RPM > 70% of RPMmax) is hardly ever used, only about 0.4%, and is mainly achieved during acceleration, or driving close to maximum speed, which does not happen in urban conditions. The average RPM value oscillates between 30÷40% of the nominal RPMmax speed. According to the study [38], a motor vehicle engine operates in the speed range of less than 50% of RPMmax almost 80% of the time of which idling accounts for about 13%. The average speed during engine braking is about 40% of RPMmax, while rapid acceleration is about 45% of RPMmax. So in summary, the car engine mainly operates in the low to medium RPM range with low to medium MAP. This means that, in the case of a car engine, only about 11.6% of the operating time is high load, and the main part of the operating time is low (about 35%) and medium (about 47.5%) load (Fig. 21). This is also confirmed by other studies [39].

Under idling conditions, the operating time of the aircraft engine was about 8.7%, i.e. more than twice as short as that of the car engine (about 14.4%) (Figure 22). Under WOT conditions, the aircraft engine had an operating time of 2.3%, while for the car engine this condition was extremely rare – about 0.1%.

The study shows that most of the time the ASz-62IR-16E aircraft engine operated in steady-state conditions, i.e. about 90% of the time. Comparing the flight results to similar studies conducted for automotive vehicles [29], a very similar share

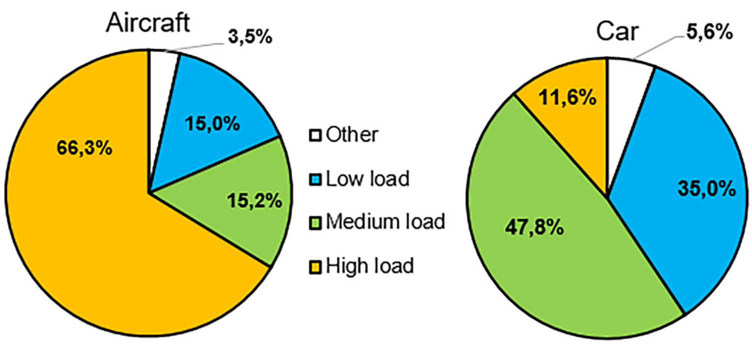

Figure 21. Aircraft and automotive engine operating times under different load conditions

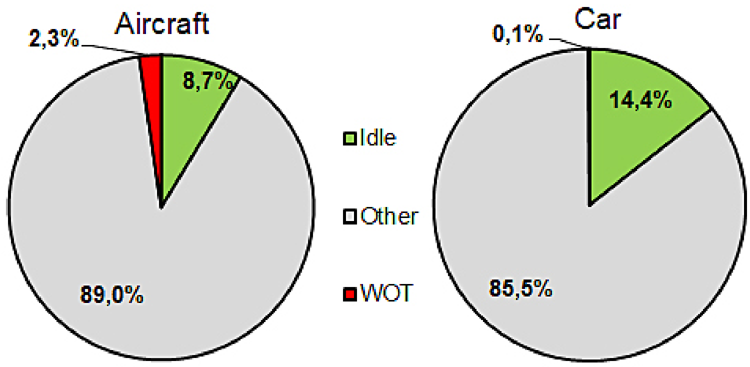

Figure 22. Aircraft and car engine operating times for IDLE, WOT and others

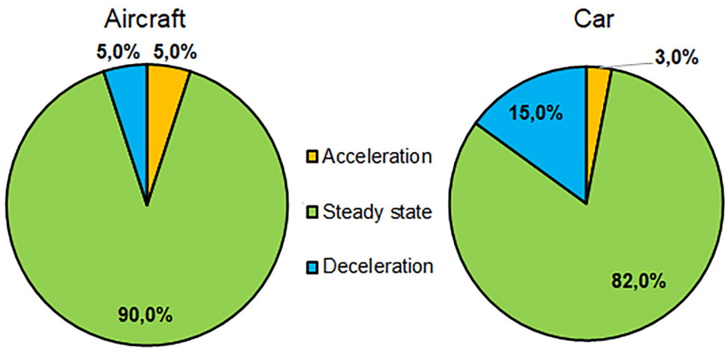

Figure 23. Comparison of the contribution of different operating states of aircraft and automotive engines

of steady-state operation can be observed. In the case of the automotive engine, steady-state operation accounts for about 82% of the operating time. (Fig. 23). This also means that the share of steady-state and transient operations of aircraft engines is very similar to that of car engines.

The difference, however, is in the proportion of acceleration and deceleration. In the case of the aircraft engine, there is an approximately similar acceleration and braking time for the engine, whereas in the case of the car engine, the braking time is approximately 5 times higher. Engine braking is not included in this analysis.

CONCLUSIONS

The paper shows that the steady-state operating conditions of an aircraft piston engine differ significantly from those of an automotive engine. Furthermore, it has been shown that the ASz-62IR-16E aircraft engine of the AN-2 under real flight conditions has a specific, most frequently used operating point lying in the range of values: RPM = 1800 ÷ 1900 min^{-1} and MAP = 88 ÷ 95 kPA. The study also showed a small number of aircraft engine operating transients. The defined aircraft engine operating transients accounted for about 10% of the total flight time, of which positive transients (acceleration) accounted for almost 5% and negative transients (deceleration just over 5% of the total flight time (Fig. 23)).

Significantly, for motor vehicles, transients (understood as acceleration, deceleration and braking) accounted for a total of almost 20% of operating time (i.e. about twice more than for an aircraft engine) with positive transients being about five times less than negative transients. This is due to a different way the driving force is transferred. During deceleration, e.g. when approaching a traffic light, the kinetic energy of the vehicle continuously drives the engine crankshaft, which keeps the negative dn/dt value for a long time. Acceleration in urban traffic, on the other hand, takes place dynamically until the required speed is reached and then speed is usually maintained. In the case of airplane propulsion, both acceleration and deceleration can be performed by rapidly varying speed to required speed and then the speed of motion is not linearly dependent on the speed of rotation, so its variation can occur while a steady- state engine operation is maintained.

REFERENCES

1. Kilikevičius A, Rimša V, Rucki M. Investigation of influence of aircraft propeller modal parameters on small airplane performance, Eksploatacja i Niezawodność, 2020; 22(1). 10.17531/ein.2020.1.1.
2. Piancastelli L, Cassani S, Calzini F, Pezzuti E. The decisive advantage of CRDID on spark-ignition piston engines for general aviation: Propeller and engine matching for a specific aircraft, ARPN J. Eng. Appl. Sci., 2018; 13(13), 4244–4252.
3. Pogačnik B, Duhovnik J, Tavčar J. Aircraft fault forecasting at maintenance service on the basis of historic data and aircraft parameters. Eksploatacja i Niezawodność, 2017; 19(4): 624–633. 10.17531/ein.2017.4.17.
4. Siadkowska K, Wendeker M, Grabowski Ł. An investigation of the fuel injector dedicated to the aircraft opposed-piston two-stroke diesel engine, Combust. Engines, 2019; 177(2): 151–155, doi: 10.19206/ce-2019-227.
5. Jakliński P. Analysis of the dual control system operation during failure conditions, Eksploatacja i Niezawodnośc – Maintenance and Reliability 2013; 15(3): 265–271. doi: dx.doi.org/10.17531/ein.
6. Eriksson L. Mean value models for exhaust system temperatures, SAE Tech. Pap., 2002; 111: 753–767, doi: 10.4271/2002-01-0374.
7. Czarnigowski J, Wendeker M, Jakliński P, Pietrykowski K, Nazarewicz A, Gęca M, Zyśka T. Testing non-uniformity of the combustion process in a radial aircraft engine, SAE Tech. Pap., 2007, doi: 10.4271/2007-01-2074.
8. Zhang K, Huang X, Xie Z, Zhou M. Design and optimization of a novel electrically controlled high pressure fuel injection system for heavy fuel aircraft piston engine, Chinese J. Aeronaut., 2018; 31(9): 1920–1928, doi: 10.1016/j.cja.2018.06.013.
9. Wang Y, Shi Y, Cai M, Xu W, Yu Q. Efficiency optimized fuel supply strategy of aircraft engine based on air-fuel ratio control, Chinese J. Aeronaut., 2019; 32(2): 489–498, doi: 10.1016/j.cja.2018.10.002.
10. Motapon NS, Dessaint LA, Al-Haddad K. A comparative study of energy management schemes for a fuel-cell hybrid emergency power system of more-electric aircraft, IEEE Trans. Ind. Electron., 2014; 61(3): 1320–1334, doi: 10.1109/TIE.2013.2257152.
11. Thoma EM, Grönstedt T, Sola EO, Zhao X. Assessment of an open-source aircraft noise prediction model using approach phase measurements, J. Aircr., 2024; 61(3), 745–760, doi: 10.2514/1.C037332.
12. Tomaszek H, Jasztal M, Zieja M, A simplified method to assess fatigue life of selected structural components of an aircraft for a variable load spectrum, Eksploat. i Niezawodn., 2011; 4: 29–34.
13. Kirmizi M, Aygun H, Turan O. Energetic and exergetic metrics of a cargo aircraft turboprop propulsion system by using regression method for dynamic flight. Energy, 2024; 296, doi: 10.1016/j.energy.2024.131153.
14. Luongo A, Nuccio P, Vignoli M. Optimization of a light aircraft spark-ignition engine, SAE Tech. Pap., 2006; 724: 776–790, doi: 10.4271/2006-01-2420.
15. Armstrong JB Simon DL. Implementation of an integrated on-board aircraft engine diagnostic architecture, 47th AIAA/ASME/SAE/ASEE Jt. Propuls. Conf. Exhib. 2011; 1–11, doi: 10.2514/6.2011-5859.
16. Yu Y, Cui W, Song B, Wang S, Evaluation of reliability growth in an unmanned aerial vehicle during successive phases of flight testing, Eksploat. i Niezawodn., 2010; 2: 43–47.
17. Sivertsson M, Sundström C, Eriksson L, Adaptive control of a hybrid powertrain with map-based ECMS, IFAC Proc. 2011; 44(1): 2949–2954, doi: 10.3182/20110828-6-IT-1002.02091.
18. Zhang R, Fujimori S. The role of transport electrification in global climate change mitigation scenarios," Environ. Res. Lett., 2020; 15: 3, doi: 10.1088/1748-9326/ab6658.
19. Mitchell G, Tsao H, Randell T, Marks J, Mackay P. Impact of electric scooters to a tertiary emergency department: 8-week review after implementation of a scooter share scheme, EMA – Emerg. Med. Australas., 2019; 31(6), 930–934, doi: 10.1111/1742-6723.13356.
20. Chen J, Wang C, Chen J, Investigation on the selection of electric power system architecture for future more electric aircraft, IEEE Trans. Transp. Electrif., 2018; 4(2): 563–576, doi: 10.1109/TTE.2018.2792332.
21. Kuźniar M. Energy comparative analysis of power units for use in light aircraft, AUTOBUSY – Tech. Eksploat. Syst. Transp., 2019; 20(1–2): 88–92, doi: 10.24136/atest.2019.013.
22. Zhang X, Chen Y, Hu J, Recent advances in the development of aerospace materials, Prog. Aerosp. Sci., 2018; 97(August 2017): 22–34, doi: 10.1016/j.paerosci.2018.01.001.
23. Orkisz M, Kuźniar M. 3E – A new paradigm for the development of civil aviation, Combust. Engines, 2020; 181(2): 3–10, doi: 10.19206/ce-2020-201.
24. Misra A. Energy storage for electrified aircraft: The need for better batteries, fuel cells, and supercapacitors, IEEE Electrif. Mag., 2018; 6(3), 54–61, doi: 10.1109/MELE.2018.2849922.
25. Zhao X, Guerrero J M, Wu X. Review of aircraft electric power systems and architectures, ENERGYCON 2014 – IEEE Int. Energy Conf., 2014; 949–953, doi: 10.1109/ENERGYCON.2014.6850540.
26. Peng W. Reliability and risk assessment of aircraft electric systems, Eksploatacja I Niezawodność,

2014; 16(4): 497.

27. Trainelli L, Perkon I, MAHEPA – A Milestone-Setting Project in Hybrid-Electric Aircraft Technology Development, 2019; 1.
28. Pornet C, Isikveren AT. Conceptual design of hybrid-electric transport aircraft, Prog. Aerosp. Sci., 2015; 79: 114–135, doi: 10.1016/j.paerosci.2015.09.002.
29. Wang Y, Du J, Zhao Q, Zhang H. Optimization design and analysis of power management for serial hybrid-electric propulsion system under aircraft/engine integrated framework, Int. J. Aeronaut. Sp. Sci., 2024; 25(2); 319–330, doi: 10.1007/s42405-023-00674-5.
30. Mashamba TM, Wen J, Spataru C, Weng Y, Lv X. characteristic investigation of a novel aircraft sofc/gt hybrid system under varying operational parameters, Appl. Sci., 2024; 14(8), doi: 10.3390/app14083504.
31. Andrych-Zalewska M, Chlopek Z, Merkisz J, Pielecha J. Research on exhaust emissions in dynamic operating states of a combustion engine in a real driving emissions test, Energies, 2021; 14(18), doi: 10.3390/en14185684.
32. Ludowicy J, Rings R, Finger D F, Braun C. Sizing studies of light aircraft with serial hybrid propulsion systems, Deutsche Gesellschaft für Luft- und Raumfahrt-Lilienthal-Oberth eV, 2018. doi: 10.25967/480226.
33. Finger DF, Braun C, Bil C. Comparative assessment of parallel-hybrid-electric propulsion systems for four different aircraft, J. Aircr. 2020; 57(5): 843–853, doi: 10.2514/1.C035897.
34. A.S. Agency and European, Data Sheet Data Sheet, 2015. [Online]. Available: http://www.papersearch.net/view/detail.asp?detail_key=10000715.
35. Aircraft Engine Installation Manual ASz-62IR-16E, Approved by EASA, Type Certificate EASA.E.140 14.06.2013; 2.
36. Ankur K, Avinash KA. Lean-burn combustion in direct-injection spark-ignition engines. Alternative Fuels and Advanced Combustion Techniques as Sustainable Solutions for Internal Combustion Engines, First Online: 16 May 2021; 186: 281–317, Accesses, Part of the Energy, Environment, and Sustainability book series, doi: 10.1007/978-981-16-1513-9_12.
37. Sharma N, Agarwal AK. Gasoline direct injection engines and particulate emissions BT – Air pollution and control, N. Sharma, A.K. Agarwal, P. Eastwood, T. Gupta, and A.P. Singh, Eds. Singapore: Springer Singapore, 2018; 87–105. doi: 10.1007/978-981-10-7185-0_6.
38. Wendeker M, Jakliński P, Czarnigowski J. Experimental anałysis of automotive engine conditions of operation. E Eksploatacja i Niezawodnosc – Maintenance and Reliability” 2000; 6: 19–28, Lublin, doi: dx.doi.org/10.17531/ein.
39. Huang Y, Surawski NC, Organ B, Zhou JL, Tang OHH, Chan FFC, Fuel consumption and emissions performance under real driving: Comparison between hybrid and conventional vehicles, Sci. Total Environ., 2019; 659: 275–282, doi: 10.1016/j.scitotenv.2018.12.349.